

Discovery of New Narrow-Band Phosphors with the UCr_4C_4 -Related Type Structure by Alkali Cation Effect

Ming Zhao, Yayun Zhou, Maxim S. Molochev, Qinyuan Zhang, Quanlin Liu, and Zhiguo Xia*

Narrow-band luminescence materials used in white light-emitting diodes (WLEDs) have demonstrated a great potential to increase the maximum accessible color gamut, improve the color rendition, or enhance the visual luminous efficacy for illumination and display devices. So far, the discovery of narrow-band rare earth doped phosphors for emerging applications remains challenging owing to the limited systems in use and the broadening effect of 4f–5d transition. Here, two narrow-band cyan-emitting phosphors with the UCr_4C_4 -related type structure, $\text{RbNa}_2\text{K}(\text{Li}_3\text{SiO}_4)_4:\text{Eu}^{2+}$ (RNKLSO:Eu²⁺) and $\text{CsNa}_2\text{K}(\text{Li}_3\text{SiO}_4)_4:\text{Eu}^{2+}$ (CNKLSO:Eu²⁺), are reported. The narrow-band emission results from the highly condensed network and a cube-like site for the activator (Eu²⁺). The emission peak assignments are investigated, and the variations of luminescence behavior with compositional changes of alkali cations are elaborated in detail. RNKLSO:8% Eu²⁺ (95% @ 250 °C of the integrated emission intensity at 25 °C) shows better thermal stability than that of CNKLSO:8% Eu²⁺ (79% @ 250 °C), which can be explained by the thermally activated crossover process represented in the configurational coordinate diagram. The optical properties of the as-fabricated WLEDs are studied and demonstrate potential with tunable properties for the full spectrum phosphor-converted LEDs. These findings in UCr_4C_4 -type phases help shedding light on new avenues for fabricating new and totally unexpected narrow-emitting phosphors with versatile applications.

crystal structure plays an important role in the discovery of targeted rare earth-doped phosphors for white light-emitting diodes (WLEDs).^[2] Many researches so far have focused on designing and investigating new solid-state phosphors with excellent luminescent properties, such as i) high luminescence quantum efficiency obtained by optimizing the synthesis and chemical conditions; ii) appropriate peak position achieved by changing the crystal structure of the host, the ion type, and the local environment of the activators; and iii) excellent thermal stability by modifying the chemical composition, introducing defects, and controlling the cation ordering, etc.^[3] Except for the requirements present above, the discovery of new narrow-band emitters remains challenging since there are limited systems with narrow-band and tunable emission reported in the references, and the broadening effect originating from the crystal field splitting is difficult to be overcome for the 4f–5d transition of Eu²⁺/Ce³⁺ activators.^[4] By far, these narrow-band phosphors can be widely used in many fields like WLEDs as backlights for liquid crystal displays (LCDs). The emission bands of

these phosphors are narrower, and the LCDs can achieve a larger color gamut since the color gamut refers to the various levels of colors that can potentially be displayed by a device; for example, wide color gamut is one of the more interesting television (TV) features making a TV look even more realistic.

1. Introduction

Phosphors, i.e., luminescence materials, are generally developed from the selected inorganic compounds and the doped activators, such as rare earth ions.^[1] The exploration of suitable host


M. Zhao, Prof. Q. L. Liu, Prof. Z. G. Xia
The Beijing Municipal Key Laboratory of New Energy Materials and Technologies
School of Materials Sciences and Engineering
University of Science and Technology Beijing
Beijing 100083, P. R. China
E-mail: xiazg@ustb.edu.cn

Y. Y. Zhou, Prof. Q. Y. Zhang, Prof. Z. G. Xia
State Key Laboratory of Luminescent Materials and Devices and Guangdong Provincial Key Laboratory of Fiber Laser Materials and Applied Techniques
South China University of Technology
Guangzhou 510641, P. R. China

Prof. M. S. Molochev
Laboratory of Crystal Physics
Kirensky Institute of Physics
Federal Research Center KSC SB RAS
Krasnoyarsk 660036, Russia

Prof. M. S. Molochev
Department of Engineering Physics and Radioelectronics
Siberian Federal University
Krasnoyarsk 660041, Russia

Prof. M. S. Molochev
Department of Physics
Far Eastern State Transport University
Khabarovsk 680021, Russia

 The ORCID identification number(s) for the author(s) of this article can be found under <https://doi.org/10.1002/adom.201801631>.

DOI: 10.1002/adom.201801631

Considering the structural issue for the discovery of rare earth phosphors with narrow-band emission, the bandwidth can be generally realized by adjusting the structural rigidity, the coordination number, and symmetry of the cation sites. Moreover, the narrow-band emission with different colors can find versatile application in the illumination and display devices. On the one hand, a narrow-band green phosphor combined with a narrow-band red phosphor and a blue (Ga, In)N chip, or with a narrow-band red phosphor, a narrow-band blue phosphor and a near UV chip can be used in the backlighting of LCDs, for example, β -SiAlON:Eu²⁺ (full width at half maximum (FWHM) \approx 55 nm, $\lambda_{em} \approx$ 540 nm), K₂SiF₆:Mn⁴⁺ (KSF:Mn⁴⁺, sharp peaks, $\lambda_{em} =$ 630 nm) with a blue (Ga, In)N chip.^[5] On the other hand, a combination of a narrow-band red phosphor with a broad band yellow or green phosphor and a blue (Ga, In)N chip can be applied to general lighting for improving the color rendering index (CRI) and enhancing the visual energy efficiency of WLEDs simultaneously, for example, Y₃Al₅O₁₂:Ce³⁺ (YAG:Ce, $\lambda_{em} \approx$ 535 nm) and Sr [LiAl₃N₄]:Eu²⁺ (FWHM \approx 50 nm, $\lambda_{em} \approx$ 650 nm) with a blue chip.^[6]

UCr₄C₄-type crystal structure plays an important role in the discovery of the narrow band phosphors, which crystallizes in the tetragonal system with the space group *I4/m*. Schnick's group first discovered the novel nitride phosphors, based on a UCr₄C₄-type structure, such as Sr[LiAl₃N₄]:Eu²⁺ and Sr[Mg₃SiN₄]:Eu²⁺ (FWHM = 43 nm, $\lambda_{em} =$ 615 nm).^[3b,7] These Eu²⁺ doped nitrides show narrow-band red emission owing to the highly condensed, rigid framework, and highly symmetric dopant sites. Very recently, based on our previous summarization and prediction in UCr₄C₄-type structure,^[1a,2b] our group reported oxide-based UCr₄C₄-type phosphors, RbLi(Li₃SiO₄)₂:Eu²⁺ (FWHM = 42 nm, $\lambda_{em} =$ 530 nm) and RbNa₃(Li₃SiO₄)₄:Eu²⁺ (RNLSo:Eu²⁺, FWHM = 22.4 nm, $\lambda_{em} =$ 471 nm), with superior luminescence properties and excellent thermal stability.^[3e,f] Huppertz and coworkers together with OSRAM Opto Semiconductors reported NaLi₃SiO₄:Eu²⁺ with an ultranarrow blue emission (FWHM = 32 nm, $\lambda_{em} =$ 469 nm), KLi₃SiO₄:Eu²⁺ with a broad-band, near warm white emission, and NaK₇[Li₃SiO₄]₈:Eu²⁺ with a yellow-green double emission (FWHM = 49 nm, $\lambda_{em} =$ 515 nm; FWHM = 138 nm, $\lambda_{em} =$ 598 nm) in the same oxide-based UCr₄C₄-type system.^[8] And all these compounds have been just given this year in the patent WO 2018/029304 A1 issued by OSRAM Opto Semiconductors.^[9] Hence, the general formula of alkali lithosilicates based on UCr₄C₄-type can be written as M₄(Li₃SiO₄)₄ (M is denoted as one, two, or more alkali metal ions in Cs, Rb, K, Na, Li with the total atoms of 4, similarly hereinafter). Generally, the highly condensed framework (the degree of condensation $\kappa = 1$, i.e., atomic ratio (Li, Si):O = 1) is formed by the vertex- and edge-sharing LiO₄ and SiO₄ tetrahedra in this type of crystal structure. All of the M cations are filled in the vierer ring channel, and some of the cations have highly symmetric cuboid-like environment which are more favorable for narrow-band emission. In addition, such a rigid structure can reduce the nonradiative relaxation effect in the excited Eu²⁺ ions and thereby reducing the bandwidth.

From the perspective of already known M₄(Li₃SiO₄)₄ (M = Cs, Rb, K, Na, Li) phosphors, the different alkali metal cations (M) in these compounds would exhibit different luminescent properties. Moreover, substitution strategy and the local structure

modification become an essential part to tune the optical properties of already known phosphors. Inspired by these facts, we synthesized the phosphors of RbNa₂K(Li₃SiO₄)₄:Eu²⁺ (RNKLSO:Eu²⁺) and CsNa₂K(Li₃SiO₄)₄:Eu²⁺ (CNKLSO:Eu²⁺), and the latter has been reported previously as a new phase.^[10] Here, starting from RbNa₃(Li₃SiO₄)₄, Na⁺ substituted by K⁺ for RNKLSO and for CNKLSO, Rb⁺ substituted by Cs⁺ and Na⁺ by K⁺. The photoluminescence (PL) spectra of RNKLSO:Eu²⁺ and CNKLSO:Eu²⁺ consist of a dominate peak at 480/485 nm with FWHM of \approx 26 nm, and a minor shoulder peak of \approx 530 nm. Clearly, compared with the emission peak at 471 nm for RNLSo:Eu²⁺ phosphor, the PL spectra of RNKLSO:Eu²⁺ and CNKLSO:Eu²⁺ show the redshift gradually with the substitution, which can be explained by the combined effect of the variation of centroid shift, crystal-field splitting and Stokes shift (SS). Moreover, we have analyzed the mechanisms on the thermal quenching behavior of RNKLSO:Eu²⁺ and CNKLSO:Eu²⁺ in detail by constructing the configurational coordination diagram. The optical properties of the fabricated LED devices were also studied. The results suggest that the RNKLSO:Eu²⁺ and CNKLSO:Eu²⁺ phosphors are promising blue-emitting candidates for application in near-UV pumped full spectrum LEDs devices.

2. Results and Discussion

Since the UCr₄C₄-type structural model leads to the highly condensed network and offers a cube-like site for the activator (Eu²⁺), RbNa₃(Li₃SiO₄)₄:Eu²⁺ has been just discovered as a new ultranarrow-band blue-emitting phosphor with potential application in LCD devices.^[3e,9] Inspired by mineral-inspired phosphor design concept, we synthesized the phosphors, RNKLSO:Eu²⁺ and CNKLSO:Eu²⁺ with the UCr₄C₄-related type structure by cation substitution (Figure 1a), and the tunable photoluminescence behavior can be realized. Figure 1b shows the X-ray diffraction (XRD) patterns of RNKLSO and CNKLSO, and almost all peaks can be indexed with the standard data of RbNa₃(Li₃SiO₄)₄ (PDF card no. 82-0818) and the reported CsNa₂K(Li₃SiO₄)₄ (PDF card no. 82-0817).^[10] To further verify the structure and the phase purity of the designed samples, we performed Rietveld refinement using the crystal structure of RbNa₃(Li₃SiO₄)₄ as starting model (Figure S1, Supporting Information), and the results show that only very small amount of Li₂SiO₃ impurity can be checked, 0.89(7)% for RNKLSO and 1.7(1)% for CNKLSO in weight, respectively. For RNKLSO as a model, there are two independent Na sites in the asymmetric part of the unit cell and both of them were occupied by Na⁺/K⁺ ions. Their occupancies were refined with linear restriction $\text{occ}(\text{K}) + \text{occ}(\text{Na}) = 1$ for each site. Preliminary refinement revealed full occupation of Na1 site by K⁺ ions and 100% occupation of Na2 site by Na⁺ ions. For CNKLSO, the Rb site was occupied by Cs⁺ ions with 100% occupation, and the Na1/Na2 sites were full occupied by K⁺/Na⁺ ions, respectively. Therefore, the model was changed according to our findings. Final refinement was both stable and gave low *R*-factors (Table 1). It is confirmed that RNKLSO and CNKLSO crystallize in a tetragonal system with space group *I4/m*, which are isostructural to RNLSo. And the unit cell volume of them is bigger than RNLSo, which is attributed to the substitution of Na⁺ (1.18 Å, coordination number (CN) = 8) and Rb⁺ (1.61 Å,

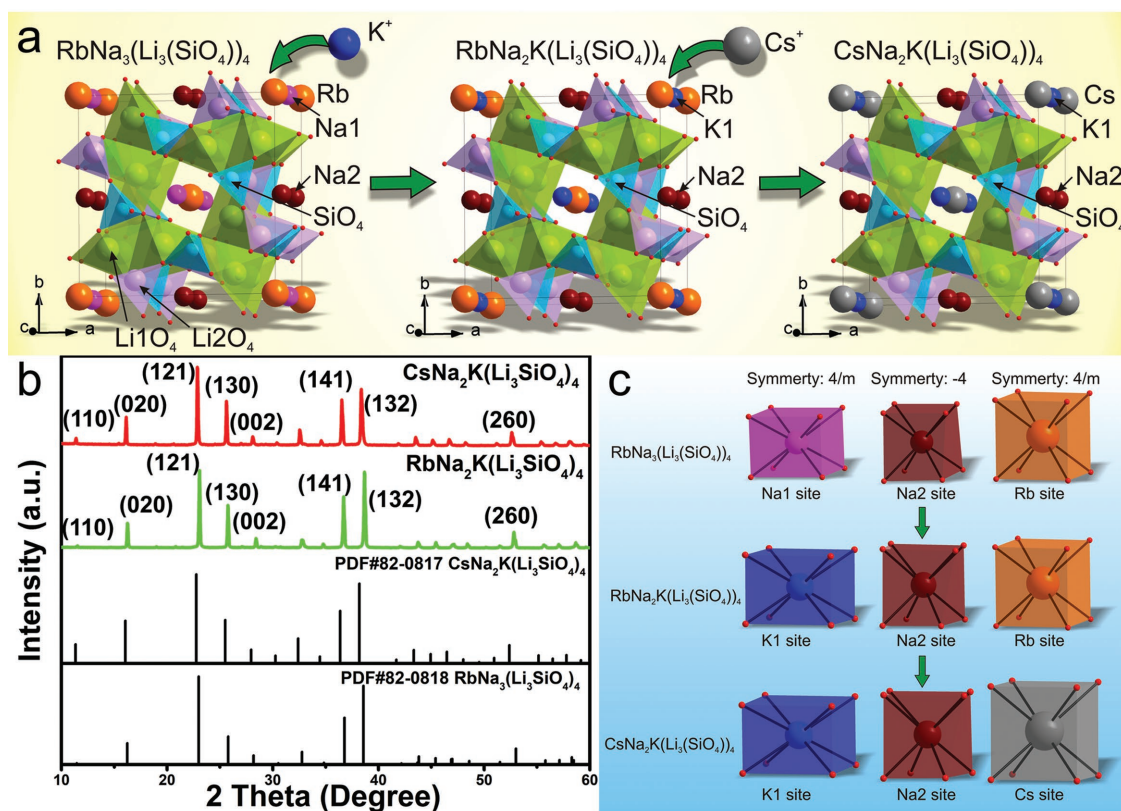


Figure 1. a) Schematic illustration of the compositions' transformation from RNLiSO to RNKLSO and to CNKLSO via cation substitution. b) XRD patterns of RNKLSO, CNKLSO, and standard patterns of PDF card no. 82-0817 for $\text{RbNa}_3(\text{Li}_3\text{SiO}_4)_4$ and PDF card no. 82-0818 for $\text{CsNa}_2\text{K}(\text{Li}_3\text{SiO}_4)_4$ as the reference. c) The coordination polyhedron of Na1, Na2, K1, Rb, and Cs sites in crystal structure of the different samples.

CN = 8) by K^+ (1.51 Å, CN = 8) and Cs^+ (1.74 Å, CN = 8) with larger ionic radius (Table 1). Coordinates of atoms and main bond lengths are shown in Tables S1 and S2 in the Supporting Information, respectively, and the crystallographic information file of RNKLSO and CNKLSO are also presented in the Supporting Information.

RNKLSO and CNKLSO share the same crystal structures, which consist of a highly condensed network of vertex- and

edge-sharing LiO_4 and SiO_4 tetrahedra with vierer ring channels in the [001] direction (Figure 1a). All of the other cations (Cs/Rb/K/Na) are filled in vierer ring channels and coordinated by eight O^{2-} ions forming ring cubic polyhedron. As shown in Figure 1c, there are two regular polyhedrons with high symmetry 4/m ($\text{RbO}_8/\text{CsO}_8$, K1O_8) and one distorted polyhedron (Na_2O_8) with relatively low symmetry -4 in RNKLSO and CNKLSO. It is reported that the high symmetry site can result in a narrow emission band compared with the low symmetry site even if it is occupied by Eu^{2+} with typical f-d transition, which is generally affected seriously by the crystal field environment.^[3b,d,e]

As can be seen from Figure 2a,e, the ^7Li NMR spectra show a similar asymmetric broad peak, and the chemical shifts are located at 4.61 ppm for RNKLSO and at 4.43 ppm for CNKLSO, respectively, which also verified that Li was incorporated in the framework. The similar two Li sites (Li1O_4 and Li2O_4) and the limited resolution of ^7Li result in the only one signal peak in the ^7Li NMR spectra, which is also similar with the value of ^7Li NMR in RNLiSO.^[3e] Scanning electron microscopy (SEM) images show that the particle sizes of RNKLSO and CNKLSO are in the range of $\approx 5\text{--}10\ \mu\text{m}$ with smooth surface (Figure 2b,c,f,g). To further support the structural analysis via the Rietveld refinement, Figure 2d,h presents the energy-dispersive X-ray spectroscopy (EDS) mapping images of the selected RNKLSO and CNKLSO particle to given more information on the chemical compositions. The

Table 1. Structure parameters of RNLiSO, and the obtained RNKLSO and CNKLSO samples.

	RNLiSO ^[3e]	RNKLSO	CNKLSO
Crystal system	Tetragonal	Tetragonal	Tetragonal
Space group	$I4/m$	$I4/m$	$I4/m$
a [Å]	10.9085(2)	10.9677(2)	10.9936(3)
c [Å]	6.3097(1)	6.2964(1)	6.3481(2)
V [Å ³]	750.83(3)	757.41(3)	767.22(5)
Z	2	2	2
R_{wp} [%]	8.48	8.01	7.49
R_{p} [%]	6.33	5.81	5.67
R_{exp} [%]	5.83	4.72	4.31
χ^2	1.45	1.70	1.74
R_{B} [%]	2.25	3.41	2.92

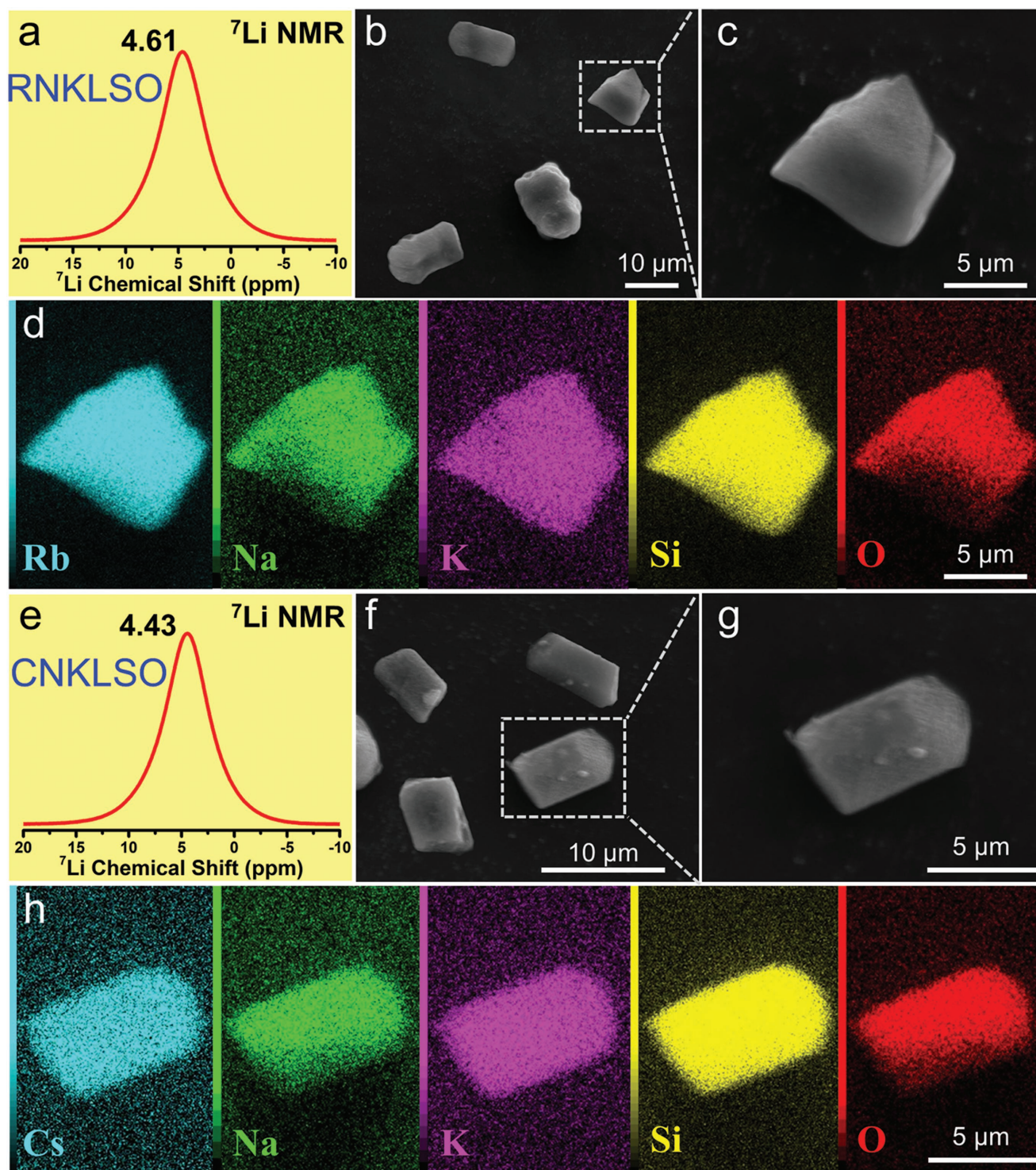


Figure 2. a,e) The ^7Li solid-state NMR spectra of RNKLSO and CNKLSO. b,f) SEM images of RNKLSO and CNKLSO particles. c,g) SEM images of the selected enlarged particles. d,h) EDS elemental mapping images of the selected RNKLSO and CNKLSO particle.

elements, including Rb/Cs, Na, K, Si, O, are homogeneously dispersed in the as-prepared particles, and the atomic ratio of Rb:Na:K:Si:O is determined as 1:1.7:1.1:4.2:15 for RNKLSO and that of Cs:Na:K:Si:O is 0.8:2:1:4.1:15 for CNKLSO. These atomic ratios are close to the formulas, $\text{RbNa}_2\text{K}(\text{Li}_3\text{SiO}_4)_4$ and

$\text{CsNa}_2\text{K}(\text{Li}_3\text{SiO}_4)_4$, which also can further verify the successful synthesis of the samples.

Figure 3a,b shows the PL spectra of RNKLSO: $x\text{Eu}^{2+}$ and CNKLSO: $x\text{Eu}^{2+}$ phosphors demonstrating the optimization of the doped Eu^{2+} contents. The results reveal that the maximum

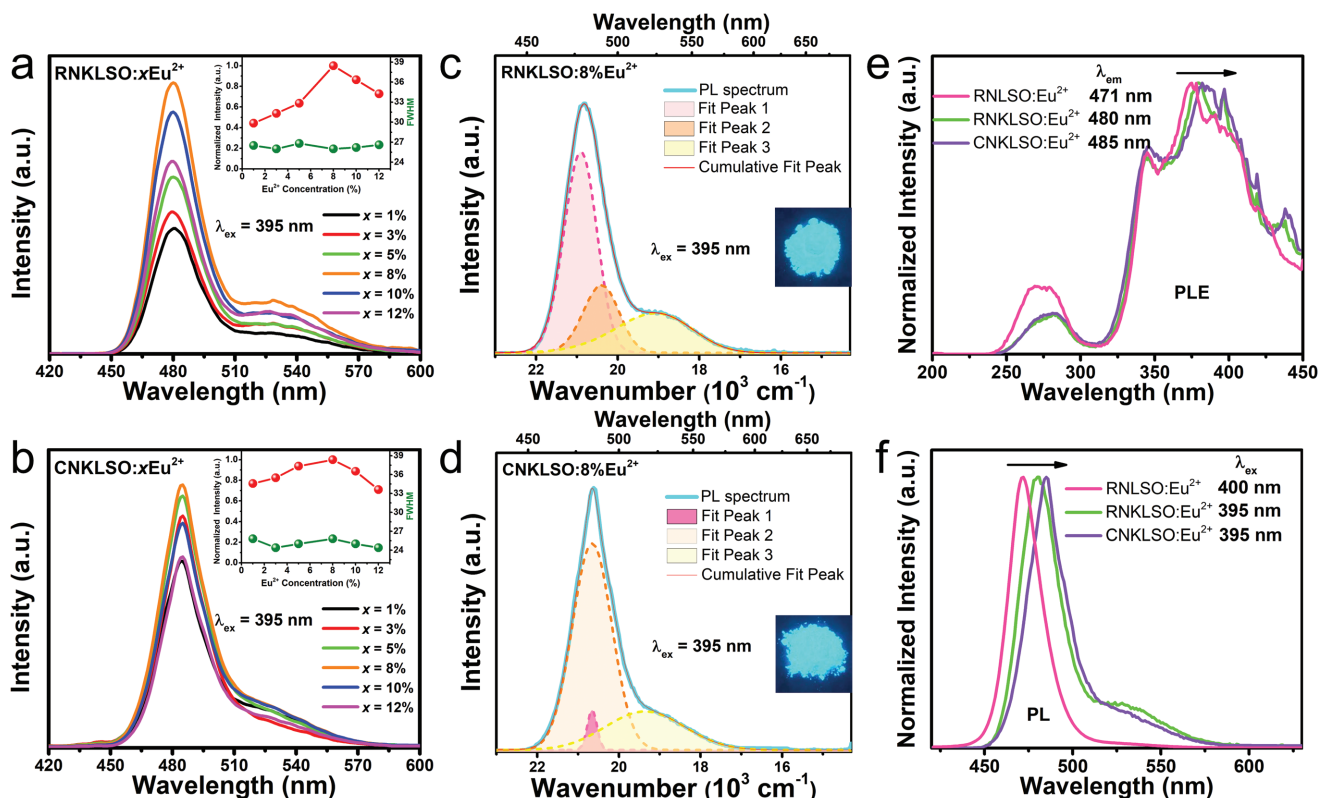


Figure 3. a, b) The PL spectra of RNKLSO: $x\text{Eu}^{2+}$ and CNKLSO: $x\text{Eu}^{2+}$ phosphors ($x = 1\text{--}12\%$). The inset shows the dependence of normalized integrated emission intensities and FWHM values on the Eu^{2+} doping concentration. c, d) The Gaussian peaks fitting of the PL spectra of RNKLSO: $8\% \text{Eu}^{2+}$ and CNKLSO: $8\% \text{Eu}^{2+}$ at room temperature. The inset shows the digital photographs of RNKLSO: $8\% \text{Eu}^{2+}$ and CNKLSO: $8\% \text{Eu}^{2+}$ phosphors under 365 nm UV lamp. e, f) The PLE and PL spectra of RNLSO: Eu^{2+} , RNKLSO: $8\% \text{Eu}^{2+}$, and CNKLSO: $8\% \text{Eu}^{2+}$ at room temperature.

emission intensity can be reached at $x = 8\%$ with the nominal content given by the designed starting materials for the two series of samples. Moreover, the measured PL spectra of the two series of samples excited at 395 nm consist of a dominate peak at 480/485 nm with FWHM of ≈ 26 nm (the inset of Figure 3a,b), and a minor shoulder broad peak of ≈ 530 nm, indicating that Eu^{2+} ions occupy distinct sites. As can be seen from Figure 3c,d, the PL spectra of RNKLSO: $8\% \text{Eu}^{2+}$ and CNKLSO: $8\% \text{Eu}^{2+}$ can be well divided into three Gaussian peaks, and the emission peaks and FWHM values are shown in Table 2. For RNKLSO: $8\% \text{Eu}^{2+}$, two narrow peaks with FWHM of ≈ 21.5 and 24.8 nm should be assigned to Eu^{2+} that enter the Rb and K1 sites with the highly cubic symmetry, and the slightly wide emission band with FWHM of ≈ 60.4 nm is attributed to that Eu^{2+} enter the Na2 sites with the low symmetry.

Table 2. Spectra data on three Gaussian fitting peaks of RNKLSO: $8\% \text{Eu}^{2+}$ and CNKLSO: $8\% \text{Eu}^{2+}$.

	RNKLSO: $8\% \text{Eu}^{2+}$		CNKLSO: $8\% \text{Eu}^{2+}$	
	λ_{em} [cm^{-1} (nm)]	FWHM [cm^{-1} (nm)]	λ_{em} [cm^{-1} (nm)]	FWHM [cm^{-1} (nm)]
Peak 1	20 901 (478.4)	940.7 (21.5)	20 657 (484.1)	279 (6.5)
Peak 2	20 395 (490.3)	1031.7 (24.8)	20 657 (484.1)	1132.8 (26.6)
Peak 3	19 070 (524.4)	2204.9 (60.4)	19 363 (516.4)	2265.7 (60.6)

This explanation can also be applied to the assignment of three Gaussian peaks of CNKLSO: $8\% \text{Eu}^{2+}$. To further verify that the emissions arise from Eu^{2+} in different lattice sites in RNKLSO: $8\% \text{Eu}^{2+}$ and CNKLSO: $8\% \text{Eu}^{2+}$, the decay curves at room temperature (RT) monitored at different wavelengths under 395 nm excitation are measured (Figure S2, Supporting Information). For RNKLSO: $8\% \text{Eu}^{2+}$, the lifetimes are evaluated to be 0.759, 0.811, and 1.049 μs monitored at 478, 490, and 524 nm, respectively. For CNKLSO: $8\% \text{Eu}^{2+}$, the lifetimes are calculated to be 0.745 and 0.906 μs monitored at 484 and 516 nm, respectively. The different lifetime values also verify the existence of different emission centers in RNKLSO: $8\% \text{Eu}^{2+}$ and CNKLSO: $8\% \text{Eu}^{2+}$.

Furthermore, the normalized photoluminescence excitation (PLE) spectra of the RNLSO: Eu^{2+} , RNKLSO: $8\% \text{Eu}^{2+}$, and CNKLSO: $8\% \text{Eu}^{2+}$ monitored at different wavelength are shown in Figure 3e. Both RNKLSO: $8\% \text{Eu}^{2+}$ and CNKLSO: $8\% \text{Eu}^{2+}$ present two main excitation bands: one minor excitation band from 250 to 300 nm and one major excitation band from 300 to 450 nm. The diffuse reflectance spectra both show two absorption bands over the 280–320 and 330–470 nm, which matched with the PLE spectra (Figure S3, Supporting Information). The key PLE spectra data of these compounds have been analyzed and listed in Table 3. The centroid position of excitation spectrum (λ_{c}) is the wavelength at which the integrated intensity of the excitation spectrum reaches half of the total integrated

Table 3. The average electronegativity χ_{av} of the cations and spectra data of RNLSO:Eu²⁺, RNKLSO:8% Eu²⁺, and CNKLSO:8% Eu²⁺.

	χ_{av}	λ_c [nm]	λ_{em} [nm]	FWHM [nm]	SS [cm ⁻¹]
RNLSO ^[3e]	1.43	378	471	22.4	–
RNKLSO	1.42	381	480	26	1998
CNKLSO	1.40	383	485	26	2212

intensity, and λ_c increases from 378 to 381 to 383 nm with the substitution of Na⁺ by K⁺ and Rb⁺ by Cs⁺. It is found that the excitation bands gradually shift toward the low-energy region but the width of the band hardly changes (Figure 3e). In general, the PLE spectrum of the Eu²⁺ f–d transition is closely associated with the centroid shift (ϵ_c) and crystal-field splitting (ϵ_{cfs}), as shown in Figure 4. On the one hand, the larger split of 5d energy level would result in the wider excitation band.^[11] Hence, we can ignore the effect of crystal-field splitting on the excitation spectra owing to the width of the band hardly changes. On the other hand, the centroid shift depends on the nephelauxetic effect, which is related to the covalency between the lanthanide ion and the anion ligands of host lattice.^[12] The centroid shift of 5d-levels of Ce³⁺ in oxides has been studied by Dorenbos.^[13] Because the optical properties of Ce³⁺ are similar to those of Eu²⁺ in the same host, the estimated value of ϵ_c for describing the characteristic of Ce³⁺ can also be applied to Eu²⁺.^[11] According to the model proposed by Morrison^[14] and development by Dorenbos,^[13] the relationship between the centroid shift ϵ_c and the anion spectroscopic polarizability α_{sp} can be demonstrated as^[13]

$$\epsilon_c = 1.79 \times 10^{13} \alpha_{sp} \sum_{i=1}^N \frac{1}{(R_i - 0.6\Delta R)^6} \quad (1)$$

where R_i is the individual bond length to the N coordinating anions in the unrelaxed lattice. $\Delta R \equiv R_M - R_{Ln}$, where R_M is the ionic radius of the cation that is replaced by the lanthanide Ln with ionic radius R_{Ln} . $0.6\Delta R$ is an estimation of the bond length relaxation. A qualitative relationship between α_{sp} and

the average cation electronegativity χ_{av} in oxide compounds was defined as^[13]

$$\alpha_{sp} = 0.4 + \frac{4.6}{\chi_{av}^2} \quad (2)$$

And the average cation electronegativity χ_{av} can be calculated by the following equation^[15]

$$\chi_{av} = \frac{1}{N_a} \sum_i^{N_c} \frac{z_i \chi_i}{\gamma} \quad (3)$$

where the summation is over all cations (N_c) in the formula of the compound, and N_a is the number of anions in the formula. A cation of formal charge $+z_i$ will bind on average with z_i/γ anions of formal charge $-\gamma$. With Pauling type^[16] electronegativity values χ_i as compiled by Allred^[17] ($\chi_{Na} = 0.93$, $\chi_K = 0.82$, $\chi_{Rb} = 0.82$, and $\chi_{Cs} = 0.79$), χ_{av} of RNLSO, RNKLSO, and CNKLSO were calculated (Table 3), and they gradually decrease. From Equations (1) and (2), it can be found that the centroid shift ϵ_c is positive relationship with the anion spectroscopic polarizability α_{sp} that is negative relation with average electronegativity χ_{av} . Hence, the decreasing of χ_{av} enables ϵ_c to enhance, which reduce the energy of 5d excited state. The corresponding redshift of the excitation band can be observed, which is consistent with the obtained PLE spectra (Figure 3e). The emission band is determined by the lowest 5d energy level and Stokes shift. The SS is defined as the energy difference between the maximum of the (lowest) excitation band and that of the emission band.^[18] It can be found that the SS gradually increases (Table 3). Hence, the redshift of the PL spectra is attributed to the reduced 5d energy level and the increased Stokes shift. Schematic energy level diagram for Eu²⁺ ions in the RNKLSO and CNKLSO crystal structure (Figure 4) shows the process for the variation of the PLE and PL spectra in detail.

The excellent thermal stability of phosphors is of great importance for high power applications. Temperature-dependent PL spectra of RNKLSO:8% Eu²⁺ and CNKLSO:8% Eu²⁺ are presented in Figure 5a–d. Both of the two samples demonstrate

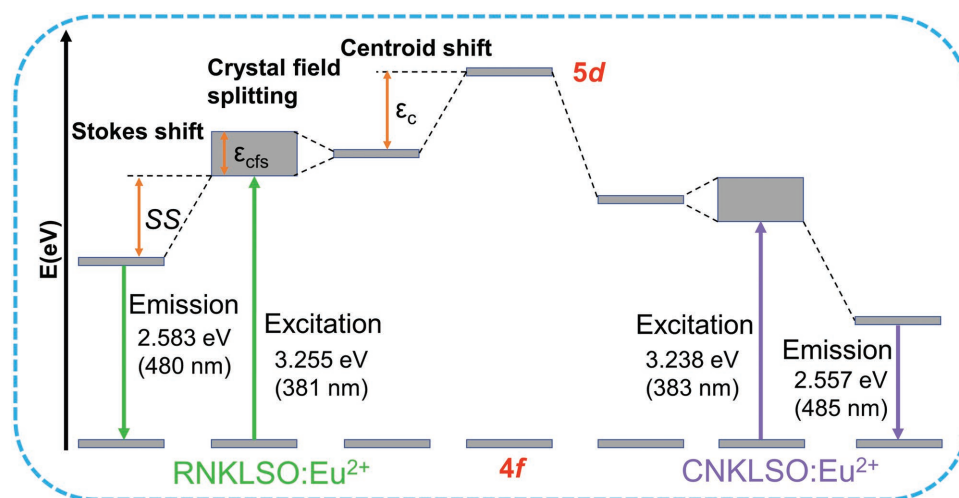


Figure 4. Schematic energy level diagram for Eu²⁺ ions in the RNKLSO and CNKLSO crystal structure.

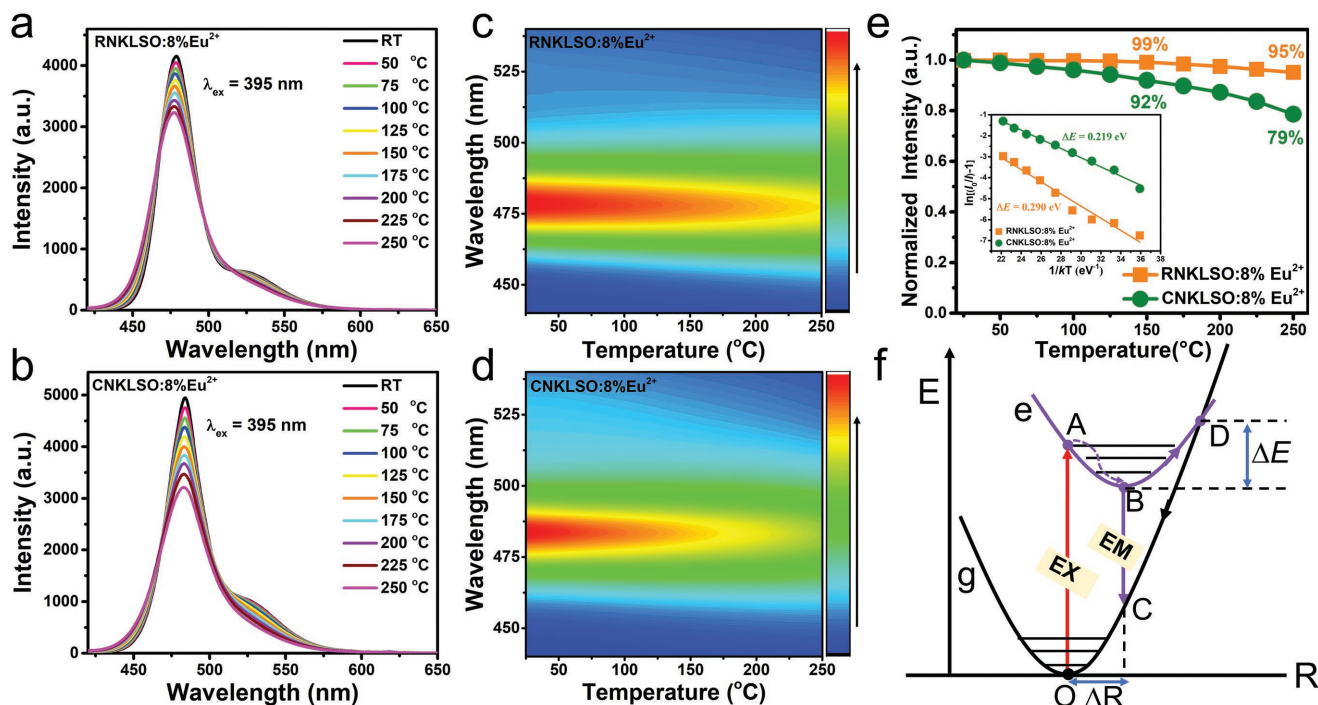


Figure 5. a,b) Temperature-dependent emission spectra of RNKLSO:8% Eu²⁺ and CNKLSO:8% Eu²⁺ phosphors under 395 nm excitation in the temperature range RT–250 °C. c,d) Thermal quenching behavior of RNKLSO:8% Eu²⁺ and CNKLSO:8% Eu²⁺ phosphors. e) Temperature-dependent normalized integrated emission intensities of RNKLSO:8% Eu²⁺ and CNKLSO:8% Eu²⁺. The inset shows the fitted activation energy for the thermal quenching of RNKLSO:8% Eu²⁺ and CNKLSO:8% Eu²⁺ phosphors using the Arrhenius equation. f) Configurational coordinate diagrams illustrating the thermally quenching of Eu²⁺ 5d–4f luminescence.

good thermal stability. Evidently, the thermal quenching of RNKLSO:8% Eu²⁺ is slower than CNKLSO:8% Eu²⁺. At 250 °C, the PL integrated intensity drops to 79% of the initial intensity at RT for CNKLSO:8% Eu²⁺ but only drops to 95% for RNKLSO:8% Eu²⁺ (Figure 5e). The PL intensity can be fitted by the Arrhenius equation^[19]

$$I_T/I_0 = [1 + A \times \exp(-\Delta E/kT)]^{-1} \quad (4)$$

where I_0 and I_T are the intensity at RT and temperature T , respectively. A is a constant, ΔE is the activation energy for thermal quenching, and k is the Boltzmann constant. ΔE is shown to decrease from 0.290 to 0.219 eV (the inset of Figure 5e), which indicates the thermal quenching is more easily after the substitution of Rb⁺ by Cs⁺. The configurational coordinate diagram can be used to explain this phenomenon, as shown in Figure 5f. Generally, under the excitation of radiation, the 4f electrons would transition to 5d excited states (line OA), then the excited electrons would relax to the lowest 5d level, and finally return to the 4f ground state through radiative transition (line BC). When the temperature rises, the luminescent center located at the excited state can reach the crossing point (line BD) and then return to the ground states (line DC), which results in the thermal quenching, also called the thermally activated crossover process.^[20] It is clear that the smaller the value of displacement between the ground and excited states (ΔR), the smaller the Stokes shift between 4f–5d absorption and 5d–4f emission and the more difficult to reach the crossing point.^[18] The Stokes shift of CNKLSO:8% Eu²⁺ is

larger than RNKLSO:8% Eu²⁺, which suggests that the thermal stability of RNKLSO:8% Eu²⁺ is better than that of CNKLSO:8% Eu²⁺. Moreover, the Stokes shift is closely related to structural rigidity.^[21] The phosphor with the larger Stokes shift has weak structural rigidity and therefore leads to more poor thermal stability.

Herein, in order to further evaluate the potential applications prospect for cyan and white LEDs, the optimized RNKLSO:Eu²⁺/CNKLSO:Eu²⁺ phosphor with or without commercial green phosphor (Sr, Ba)₂SiO₄:Eu²⁺ and red phosphor CaAlSiN₃:Eu²⁺ were well-mixed with epoxy and coated on the near-UV chips ($\lambda = 395$ nm). The photoelectric parameters of LEDs are listed in Table S3 in the Supporting Information. Both of the emission spectra of prepared single-color LED-1 (RNKLSO:Eu²⁺) and LED-2 (CNKLSO:Eu²⁺) consisting of two emission bands and emitted an intensive cyan light seen with the naked eyes (Figure 6a), and the Commission Internationale de L'Eclairage (CIE) chromatic coordinates are of (0.126, 0.281) and (0.119, 0.311), respectively (Table S3, Supporting Information). These cyan phosphors are suitable candidates for increasing the blue component of the WLEDs to realize the full spectrum emission application. The fabricated WLEDs of LED-3 (RNKLSO:Eu²⁺) and LED-4 (CNKLSO:Eu²⁺) glow bright warm white light with the spectra extending the entire visible region (Figure 6b), with a low correlated color temperature (CCT) of 3707 and 3331 K, as well as the CIE chromaticity coordinates locating on the Planckian locus (Figure 6c), respectively. From the current results, RNKLSO:Eu²⁺/CNKLSO:Eu²⁺ phosphors are expected to be successfully used in single cyan

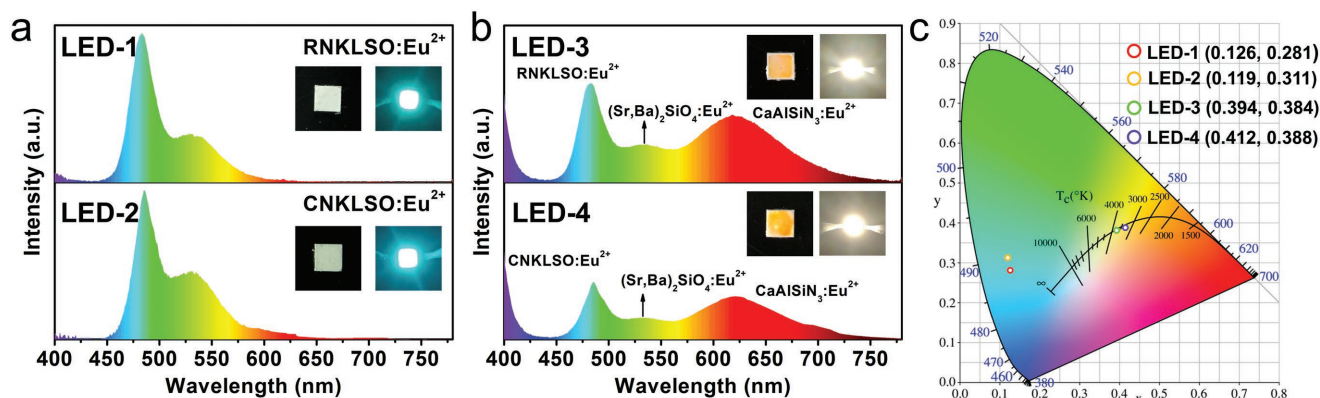


Figure 6. a,b) Emission spectra of cyan and white LEDs fabricated by RNKLSO:Eu²⁺/CNKLSO:Eu²⁺, with or without commercial green phosphor (Sr, Ba)₂SiO₄:Eu²⁺ and red phosphor CaAlSiN₃:Eu²⁺ on a near-UV LED chip ($\lambda = 395$ nm) under a current of 60 mA. The inset shows the photographs of their corresponding LEDs. c) CIE chromaticity diagram of the fabricated LEDs.

LEDs or near-UV WLEDs to fulfill the requirement of the full spectrum illumination.

3. Conclusion

In summary, we successfully prepared the RNKLSO:Eu²⁺ and CNKLSO:Eu²⁺ phosphors which are isostructural to RNLSo:Eu²⁺. RNKLSO:Eu²⁺ exhibits a narrow-band cyan emission at 480 nm with FWHM of 26 nm, and CNKLSO:Eu²⁺ also shows a narrow-band cyan emission ($\lambda_{em} = 485$ nm, FWHM = 26 nm). With the substitution of Na⁺ by K⁺ and Rb⁺ by Cs⁺, the excitation band shows a redshift owing to the increased centroid shift. The emission peak is tuned from blue (RNLSo:Eu²⁺) to cyan (RNKLSO:Eu²⁺ and CNKLSO:Eu²⁺), and the redshift of the emission spectrum can be ascribed to the combined effect of the reduced 5d energy level and the increased Stokes shift. RNKLSO:Eu²⁺ phosphor exhibits smaller thermal quenching than that of CNKLSO:Eu²⁺ and the configurational coordinate diagram is used to understand the mechanism for the thermal quenching behavior. Furthermore, the performance of LEDs indicates that the cyan phosphors RNKLSO:Eu²⁺ and CNKLSO:Eu²⁺ are promising candidates for near-UV single cyan LEDs and WLEDs light sources for advanced full spectrum illumination.

4. Experimental Section

Materials and Preparation: The powder samples of RNKLSO:*x*Eu²⁺ (*x* = 0–12%) and CNKLSO:*x*Eu²⁺ (*x* = 0–12%) were prepared by a conventional solid-state reaction. The starting materials, including Cs₂CO₃ (A.R., Aladdin), Rb₂CO₃ (A.R., Aladdin), K₂CO₃ (A.R., Aladdin), Na₂CO₃ (A.R., Aladdin), Li₂CO₃ (A.R., Aladdin), SiO₂ (A.R., Aladdin), and Eu₂O₃ (99.99%, Aladdin), were weighted in stoichiometric ratios and homogeneously mixed in an agate mortar with an appropriate ethanol as the solvent. The powder mixtures were placed in aluminum oxide crucibles and sintered at 550 °C for 5 h in air, then reground into fine powders and sintered three times at 750 °C for 4 h under a reducing atmosphere (N₂/H₂ = 90%/10%) in a tube furnace. Finally, the samples were cooled to room temperature naturally and ground for further measurements.

Characterization: The powder XRD measurements of RNKLSO:*x*Eu²⁺ and CNKLSO:*x*Eu²⁺ at room temperature were performed on a Bruker

D8 ADVANCE diffractometer with monochromatized Cu K α radiation ($\lambda = 1.5406$ Å) at 40 kV and 40 mA. Rietveld refinement was conducted by using TOPAS 4.2. The ⁷Li solid-state NMR spectrum was measured on JNM-ECZ600R at 12 kHz and the external reference was LiCl. SEM and EDS measurements of the samples were conducted on JEOL JSM-6510. The diffuse reflectance spectra at room temperature were recorded by a Hitachi UH4150 US-vis-near-infrared spectrophotometer and using white BaSO₄ for calibration. The PL and PLE spectra at room temperature were measured using an Edinburgh FLS920 fluorescence spectrophotometer equipped with the Xe900 lamp as the excitation source. The temperature-dependent spectra were measured by a Hitachi F-4600 fluorescence spectrophotometer with a heating apparatus as heating source and a 150 W Xe lamp as the excitation source. The phosphor powders were heated to 250 °C in a 25 °C interval at a heating rate of 100 °C min⁻¹ and held at each temperature for 10 min for thermal equilibrium.

LED Fabrication: LEDs were fabricated by combining the phosphors (RNKLSO:8% Eu²⁺/CNKLSO:8% Eu²⁺, with or without commercial green phosphor (Sr, Ba)₂SiO₄:Eu²⁺) and red phosphor (CaAlSiN₃:Eu²⁺) and a near-UV chip ($\lambda = 395$ nm). The proper amounts of phosphors were added into the epoxy resins and mixed thoroughly. The obtained mixture was coated on the LED chips. The photoelectric properties, including the emission spectra, CCT, CRI (*R_a*), luminous efficacy, and CIE color coordinates of the LEDs, were measured by using an integrating sphere spectroradiometer system (ATA-1000, Everfine).

Supporting Information

Supporting Information is available from the Wiley Online Library or from the author.

Acknowledgements

M.Z. and Y.Y.Z. contributed equally to this work. This work was supported by the National Natural Science Foundations of China (Grant Nos. 51722202, 91622125, and 51572023) and Natural Science Foundations of Beijing (2172036). M.S.M. acknowledges the support of the Russian Foundation for Basic Research (No. 17-52-53031).

Conflict of Interest

The authors declare no conflict of interest.

Keywords

narrow-band emission, phosphors, photoluminescence, substitution strategy, white light-emitting diodes

Received: November 25, 2018

Revised: December 19, 2018

Published online: January 2, 2019

- [1] a) Z. G. Xia, Q. L. Liu, *Prog. Mater. Sci.* **2016**, *84*, 59; b) X. Qin, X. W. Liu, W. Huang, M. Bettinelli, X. G. Liu, *Chem. Rev.* **2017**, *117*, 4488.
- [2] a) J. Meyer, F. Tappe, *Adv. Opt. Mater.* **2015**, *3*, 424; b) Z. G. Xia, Z. H. Xu, M. Y. Chen, Q. L. Liu, *Dalton Trans.* **2016**, *45*, 11214.
- [3] a) L. Huang, Y. W. Zhu, X. J. Zhang, R. Zou, F. J. Pan, J. Wang, M. M. Wu, *Chem. Mater.* **2016**, *28*, 1495; b) P. Pust, V. Weiler, C. Hecht, A. Tucks, A. S. Wochnik, A. K. Henss, D. Wiechert, C. Scheu, P. J. Schmidt, W. Schnick, *Nat. Mater.* **2014**, *13*, 891; c) S. X. Li, L. Wang, D. Tang, Y. Cho, X. Liu, X. Zhou, L. Lu, L. Zhang, T. Takeda, N. Hirotsaki, R.-J. Xie, *Chem. Mater.* **2018**, *30*, 494; d) P. Strobel, T. de Boer, V. Weiler, P. J. Schmidt, A. Moewes, W. Schnick, *Chem. Mater.* **2018**, *30*, 3122; e) H. X. Liao, M. Zhao, M. S. Molokeev, Q. L. Liu, Z. G. Xia, *Angew. Chem.* **2018**, *130*, 11902; f) M. Zhao, H. X. Liao, L. X. Ning, Q. Y. Zhang, Q. L. Liu, Z. G. Xia, *Adv. Mater.* **2018**, *30*, 1802489.
- [4] A. Meijerink, *Sci. China Mater.* **2018**, <https://doi.org/10.1007/s40843-018-9370-4>.
- [5] L. Wang, X. J. Wang, T. Kohsei, K. Yoshimura, M. Izumi, N. Hirotsaki, R. J. Xie, *Opt. Express* **2015**, *23*, 28707.
- [6] J. H. Oh, Y. J. Eo, H. C. Yoon, Y.-D. Huh, Y. R. Do, *J. Mater. Chem. C* **2016**, *4*, 8326.
- [7] S. Schmiechen, H. Schneider, P. Wagatha, C. Hecht, P. J. Schmidt, W. Schnick, *Chem. Mater.* **2014**, *26*, 2712.
- [8] D. Dutzler, M. Seibald, D. Baumann, H. Huppertz, *Angew. Chem., Int. Ed.* **2018**, *57*, 13676.
- [9] M. Seibald, D. Baumann, T. Fiedler, S. Lange, H. Huppertz, D. Dutzler, T. Schroder, D. Bichler, G. Plundrich, S. Peschke, H. Gregor, G. Achraimer, K. Wurst (OSRAM GmbH, Germany), *Patent WO 2018/029304 A1*, **2018**.
- [10] J. Hoffmann, R. Brandes, R. Hoppe, Z. *Anorg. Allg. Chem.* **1994**, *620*, 1495.
- [11] T. Wang, Q. C. Xiang, Z. G. Xia, J. Chen, Q. L. Liu, *Inorg. Chem.* **2016**, *55*, 2929.
- [12] D. P. Cui, Z. Song, Z. G. Xia, Q. L. Liu, *Inorg. Chem.* **2017**, *56*, 11837.
- [13] P. Dorenbos, *J. Lumin.* **2013**, *135*, 93.
- [14] C. A. Morrison, *J. Chem. Phys.* **1980**, *72*, 1001.
- [15] P. Dorenbos, *Phys. Rev. B* **2002**, *65*, 235110.
- [16] L. Pauling, *The Nature of the Chemical Bond*, Cornell University, New York **1960**.
- [17] A. L. Allred, *J. Inorg. Nucl. Chem.* **1961**, *17*, 215.
- [18] G. Blasse, B. C. Grabmaier, *Luminescent Materials*, Springer-Verlag, Berlin **1994**.
- [19] S. Bhushan, M. Chukichev, *J. Mater. Sci. Lett.* **1988**, *7*, 319.
- [20] a) M. M. Shang, S. S. Liang, N. R. Qu, H. Z. Lian, J. Lin, *Chem. Mater.* **2017**, *29*, 1813; b) L. X. Ning, X. W. Ji, Y. Y. Dong, W. Jin, Y. C. Huang, Z. F. Pan, P. A. Tanner, *J. Mater. Chem. C* **2016**, *4*, 5214.
- [21] K. A. Denault, J. Brgoch, S. D. Kloss, M. W. Gaultois, J. Siewenie, K. Page, R. Seshadri, *ACS Appl. Mater. Interfaces* **2015**, *7*, 7264.